Science of the Total Environment 937 (2024) 173370

Contents lists available at ScienceDirect

Science of the Total Environment

journal homepage: www.elsevier.com/locate/scitotenv

Coupling physiochemical adsorption with biodegradation for enhanced removal of microcystin-LR in water

Shengyin Tang [a,b], Lixun Zhang [a,b], Haoxin Zhu [a], Sunny C. Jiang [a,*]

[a] Department of Civil and Environmental Engineering, University of California, Irvine, 92697, United States
[b] Institute of Environment and Ecology, Tsinghua Shenzhen International Graduate School, Tsinghua University, Shenzhen 518055, China

HIGHLIGHTS

- Coupled adsorption and biodegradation enhanced MC-LR removal performance.
- Mesopore was the most dominant positive contributor to MC-LR adsorption capacity.
- Pore structure was the key factor for MC-LR biological removal.
- Pinewood-based adsorbents exhibited the best MC-LR removal performance.

GRAPHICAL ABSTRACT

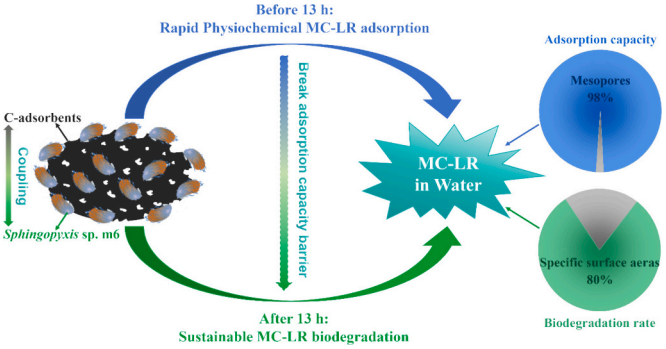

ARTICLE INFO

Editor: Jay Gan

Keywords:
Microcystin-LR
Carbonaceous adsorbents
Sphingopyxis sp. m6
Variance partitioning analysis
Water treatment

ABSTRACT

To innovate the design of water treatment technology for algal toxin removal, this research investigated the mechanisms of cyanotoxin microcystin-LR (MC-LR) removal by a coupled adsorption-biodegradation. Eight types of woody carbonaceous adsorbents with and without *Sphingopyxis* sp. m6, a MC-LR degrading bacterium, were tested for MC-LR removal in water. All adsorbents showed good adsorption capability, removing 40 % to almost 100 % of the MC-LR (4.5 mg/L) within 48 h in batch experiments. Adding *Sphingopyxis* sp. m6 continuously promoted MC-LR biological removal, and successfully broke the barrier of adsorption capacity of tested adsorbents, removing >90 % of the MC-LR in most of the coupled adsorption-biodegradation tests, especially for those adsorbents had low physiochemical adsorption capacity. Variance partitioning analysis indicated that mesopore was the dominant contributor to adsorption capacity of MC-LR in pure adsorption treatments, which acted synergistically with electrical conductivity, polarity and total functional groups on the absorbent. Pore structure was the key factor beneficial for the growth of *Sphingopyxis* sp. m6 (51% contribution) and subsequent MC-LR biological removal rate (80 % contribution). Overall, pinewood-based carbonaceous adsorbents (especially pinewood activated carbon) exhibited the highest adsorption capacity towards MC-LR and provided the most favorable conditions for biological removal of MC-LR, largely because of their high mesopore volume, total functional groups and electric conductivity. The research outcomes not only deepened the quantitative

* Corresponding author.
E-mail address: sjiang@uci.edu (S.C. Jiang).

https://doi.org/10.1016/j.scitotenv.2024.173370
Received 28 February 2024; Received in revised form 16 May 2024; Accepted 17 May 2024
Available online 19 May 2024

understanding of mechanisms for MC-LR removal by the coupled process, but also provided theoretical basis for future materials' selection and modification during the practical application of coupled process.

1. Introduction

Water eutrophication and harmful algal blooms remain important challenges to water quality and drinking water safety all over the world (Wurtsbaugh et al., 2019). Microcystin-LR (MC-LR), a type of secondary metabolites of cyanobacteria, is the most frequently detected toxin during the algal blooms in surface freshwaters (Rastogi et al., 2014). MC-LR is of worldwide distribution and bioaccumulate, which poses significant ecological and human health risks (Zhang et al., 2021). To ensure drinking water safety and protect human health, the World Health Organization (WHO) has set a provisional guideline of <1.0 μg/L of MC-LR in drinking water (WHO, 2020). However, most drinking water treatment plants, including those in the developed countries such as United States, are unprepared to manage the toxin in source water that could be 100 to 1000 times higher than the safety guidelines during and/or after algal blooms (B.-L. Liu et al., 2021).

Due to the chemical stability, high aqueous solubility and biological toxicity, MC-LR removal presents a challenge to conventional water treatment processes (Pavagadhi et al., 2013; Zeng and Kan, 2022). Advanced oxidation (AOPs) (Li et al., 2023; Park et al., 2017b), adsorption (Park et al., 2017a; Zeng and Kan, 2021) and biodegradation (Wei et al., 2023; Yang et al., 2020) have been explored to remove MC-LR from water. Adsorption by various carbon-based adsorbents, such as activated carbon and biochar, have been widely researched for removing MC-LR from water (Li et al., 2018). However, the industrial application of these carbonaceous adsorbents is still limited due to the quick saturation of the adsorption capacity. Thermal treatment (Dutta et al., 2019), solvent extraction (Nunes et al., 2021), microwave irradiation (Foo and Hameed, 2012) and microbiological regeneration (Salvador et al., 2015) are currently the main strategies for adsorption sites regeneration (Dai et al., 2019). Most of the methods require off-line operations to replace the adsorbents.

The goal of this research is to use special functional microorganisms as a low cost and eco-friendly method to couple with carbonaceous adsorbents for regeneration of adsorption sites in situ during water treatment. Previous research has shown that *Sphingopyxis* strains isolated from lake waters have high biodegradative capabilities for various organic contaminants (Sharma et al., 2021). Multiple *Sphingopyxis* strains (e.g., *Sphingopyxis* sp. YF1 (Wei et al., 2023; Yang et al., 2020), *Sphingopyxis* sp. USTB-05 (Xiao et al., 2011; Yan et al., 2012) and *Sphingopyxis* sp. m6 (Ding et al., 2018; Zhang et al., 2023)) have been shown to degrade MC-LR effectively with no harmful by-products. However, the biodegradation removal rate of MC-LR by these special functional microorganisms is much slower than the physiochemical adsorption removal rate achieved by carbonaceous adsorbents. The practical application of these special functional microorganisms is still restricted by their application requirements, including essential nutrient supplements, suitable growth conditions, long adaptation phase for optimal microbial activity and slow biodegradation rate (Salvador et al., 2015; Sharma et al., 2021).

Coupling carbonaceous material adsorption with special functional microorganisms' biodegradation may provide a novel way to achieve more efficient removal of MC-LR in long term operation and to overcome shortcomings of both isolated biodegradation and adsorption. In this research, eight types of carbonaceous adsorbents (i.e., activated carbon and biochar derived from woody materials) representing commonly used carbonaceous adsorbents in water treatment were examined in a coupling study. *Sphingopyxis* sp. m6, a well-characterized MC-LR degrading bacterium, was used in engineering of coupled adsorption-biodegradation system for MC-LR removal in water. The research outcomes deepened the quantitative understanding of mechanisms for MC-LR removal by the coupled process and provided theoretical basis for future materials' selection and modification during the application of coupled adsorption and biodegradation process.

2. Materials and methods

2.1. Preparation and characterization of carbonaceous adsorbents

Eight types of high-quality commercial carbonaceous adsorbents (i.e., the most common and best-selling bamboo-, coconut shell-, oakwood-, pinewood-based activated carbon and biochar in the U.S. market) were chosen to represent the most used woody carbonaceous adsorbents in water treatment. These commercial carbonaceous adsorbents were purchased from Amazon (https://www.amazon.com) or Etsy (https://www.etsy.com). Their commercial functions and physical shapes upon receiving are listed in Table 1. All materials received from vendors were first dried in oven at 105 °C, grinded to pass through a 100-mesh sieve before material characterization and MC-LR removal experiments.

The ash contents of the adsorbents were determined according to the latest international standard methods (ASTM D1762–84(2021)) (ASTM, 2021). The contents of carbon (C), hydrogen (H) and nitrogen (N) were directly measured by an elemental analyzer (EL Cube, Elementa, Germany) following manufacturer's protocols. The oxygen (O) contents were calculated by the difference between total mass and the sum of ash, C, H, N (Wei and Lu, 2021).

Pore characteristics and specific surface area of adsorbents were determined by measuring N_2 adsorption-desorption isotherms using a volumetric adsorption instrument (BELSORP-max, BEL, Japan). The specific surface area (S_{BET}) and mean pore width (W) were calculated through Brunauer-Emmet-Teller (BET) model. The pore characteristics including the micropore (pores width $\leq$ 2 nm) surface area (S_{micro}), mesopore (2 nm < pores width $\leq$ 50 nm) surface area (S_{meso}), total pore volume (PV_{total}), micropore volume (PV_{micro}) and mesopore volume (PV_{meso}) were calculated through Non Localized Density Functional Theory and Grand Canonical Monte Carlo method (NLDFT/GCMC).

The surface charges of the adsorbents and *Sphingopyxis* sp. m6 in M9 mineral media were measured by a zeta potential analyzer (Nano ZS, Malvern, UK). The surface functional groups were detected by Boehm titration (Bardestani and Kaliaguine, 2018; Huang et al., 2020). The electrical conductivity (EC) and pH were measured according to the

Table 1
Basic information of eight commercial carbonaceous adsorbents.

Carbonaceous adsorbents[a]	Raw materials	Types	Commercial functions	Shapes
BAW	Bamboo	Activated carbon	Water purification	Chips
BBA	Bamboo	Biochar	Air purification	Chips
CAA	Coconut shell	Activated carbon	Air purification	Granules
CAW	Coconut shell	Activated carbon	Water purification	Granules
OAW	Oakwood	Activated carbon	Water purification	Sticks
OBS	Oakwood	Biochar	Soil amendment	Chips
PAA	Pinewood	Activated carbon	Air purification	Chips
PBS	Pinewood	Biochar	Soil amendment	Chips

[a] Carbonaceous adsorbents are named by the raw material as the first letter, i.e., B is for Bamboo; the second letter represents treatments used to produce the type of adsorbent, i.e., A is for Activated carbon; the last letter is the material function defined by the commercial vendor, i.e., W is for water purification.

latest International Biochar Initiative (IBI) Biochar Standards (IBI-STD-2.1 (2015)) (Initiative, 2015).

2.2. Batch MC-LR adsorption experiments

Batch experiments, in 15 mL glass tubes, were carried out to measure MC-LR adsorption by different adsorbents in M9 minimal media (see Table S1 for compositions). MC-LR (MilliporeSigma™, Burlington, United States) stock solution (40 mg/L, protected from light) and adsorbents stock suspensions (8.0 g/L) were prepared in sterile M9 media and dispersed completely by shaking for 24 h. All experimental trials contained 0.4 g/L adsorbents. The initial concentrations of MC-LR were set according to the adsorption capacities of different adsorbents towards MC-LR based on preliminary test results. The adsorption experiments were carried out at 25 °C for 24 h in a shaker incubator. At the end of the adsorption, the mixtures were filtered through a 0.22 μm pore-size PES filter for MC-LR detection in the filtrate. The concentration of MC-LR was detected by a Quattro Premier XE UPLC-MS/MS instrument (Waters™, Milford, MA) as described in the previous research (Zhang et al., 2023).

2.3. Coupled adsorption and biodegradation for MC-LR removal

Sphingopyxis sp. m6, a well characterized MC-LR degrader, was activated from a frozen stock in Luria Bertani broth (LB, see Table S2 for composition) at 25 °C. The bacterial cells were then pelleted by centrifugation and washed by M9 media three times to remove LB. The cell pellet was finally resuspended in M9 media, a minimal media that contains the essential minerals to support the growth of *Sphingopyxis* sp. m6 in the presence of MC-LR. The bacterial concentration was adjusted to OD_{600} of 0.40 ± 0.02 before used in experimental trials according to a previous study (Zhang et al., 2023).

Coupling *Sphingopyxis* sp. m6 with the adsorbents was achieved by adding 2 mL of adsorbent stock suspension (3.0 g/L) to 10 mL of bacterial suspension in a 100 mL conical flask. The mixture was shaken at 25 °C for 12 h to allow the bacteria attachment to the carbonaceous adsorbents. At the end of the incubation, 3 mL of MC-LR stock solution was added to the mixture for assessing MC-LR removal kinetics in a total volume of 15 mL.

Initial MC-LR concentration of 4.5 mg/L was used in the kinetics study. In the repeated experiments, the initial MC-LR concentrations was increased to 30 mg/L and 15 mg/L for PAA and PBS kinetics study, respectively, because their much greater adsorption capacities towards MC-LR. All flasks containing the same concentration of adsorbent (0.4 g/L) and *Sphingopyxis* sp. m6 were shaken in 180 rpm at 25 °C for 48 h. 0.5 mL of sub-samples were collected from each flask at 0, 5 min, then 1, 3, 5, 7, 10, 13, 18, 24, 32, 40, 48 h for MC-LR analysis. The bacterial concentrations in the mixtures were determined at 0 and 32 h by plating on LB agar plate. The control experiments were also conducted to detect the MC-LR removal kinetics by carbonaceous adsorbents adsorption only or pure *Sphingopyxis* sp. m6 biodegradation only in M9 media. All the experiments were conducted in triplicate.

2.4. Data analysis

All MC-LR adsorption isotherms were fitted by Freundlich model (SI Section 1.1) (Li et al., 2018; Tseng and Wu, 2008). The adsorption distribution coefficient (K_d) was calculated according to Eq. (2) as described in SI Section 1.1 (Li et al., 2018). The MC-LR adsorption and biodegradation removal kinetics were fitted by pseudo second order kinetic model (SI Section 1.2) and first order kinetic model (SI Section 1.3), respectively (Zhang et al., 2023).

The relationship between the physiochemical properties of adsorbents (including W, PV_{total}, PV_{micro}, PV_{meso}, S_{BET}, S_{micro}, S_{meso}, total groups, acidic groups, carboxylic groups, phenolic groups, lactonic groups, basic groups, ash, C, H, N, O, (N + O)/C, O/C, H/C, zeta potential, EC) and MC-LR removal performance (K_F, n, q_e, k_2, sp. m6–32, sp. m6-q_e, sp.m6-k_2, sp.m6-k_1) were analyzed by spearman correlation coefficient using Origin2021®.

The quantitative contributions of significantly related factors of adsorbents properties to MC-LR removal performance and the growth of *Sphingopyxis* sp. m6 were analyzed by variance partitioning analysis (VPA). Specifically, the significantly related factors of adsorbents properties were first identified according to the results of spearman correlation analysis ($|r| \geq 0.5$). The factors were then analyzed by redundancy analysis using Canoco5 (Canoco5.com). The collinearity of the significantly related factors ($p \leq 0.05$) was further diagnosed using IBM SPSS® Statistics 27. Finally, no more than four significantly related factors with variance inflation factor (VIF) lower than 10 were determined as the key factors for VPA. VPA was conducted using RStudio® with "Vegan" package.

3. Results and discussions

3.1. MC-LR removal performance

3.1.1. Adsorption isotherms of MC-LR on pure adsorbents

MC-LR adsorption isotherms for the eight pure adsorbents were well fitted by Freundlich model ($R^2 \geq 0.97$) (Fig. 1). The fitting parameters (K_F and n) of Freundlich model varied widely for different adsorbents. K_F of pinewood adsorbents was higher than coconut shell adsorbents, followed by oakwood adsorbents and then bamboo adsorbents, suggesting pinewood adsorbents have the highest MC-LR adsorption capacity (Li et al., 2018; Tran, 2022). According to the K_d value (SI Section 1.1) at the same C_e of 1.0 mg/L, MC-LR adsorption capability of the adsorbents followed the order of PAA (70.24 L/g) > PBS (13.01 L/g) > CAW (11.62 L/g) > CAA (9.89 L/g) > OBS (4.15 L/g) ≈ OAW (4.11 L/g) > BAW (3.68 L/g) ≈ BBA (3.68 L/g).

The n values of the eight carbonaceous adsorbents ranged from 1.09 (BAW) to 5.27 (PBS), indicating that all adsorbents had good adsorption affinity towards MC-LR (Li et al., 2018; Tseng and Wu, 2008). PBS had the highest affinity according to the highest n value (Kano et al., 2000; Tseng and Wu, 2008). The $1/n$ values of PBS (0.19) and PAA (0.23) were markedly lower than others (0.64–0.92), implying outstanding adsorption capacity of PBS and PAA. Overall, pinewood adsorbents exhibited the best adsorption performance towards MC-LR.

3.1.2. Coupled adsorption-biodegradation enhanced MC-LR removal

Before coupling with MC-LR degrading bacteria, eight adsorbents showed significant different MC-LR removal kinetics (Fig. 2). At the same initial MC-LR concentration of 4.5 mg/L, BBA had the lowest MC-LR removal of 16.62 %, followed by BAW (32.86 %), then OAW (48.84 %) and OBS (48.55 %) after 1 h adsorption. CAA and CAW removed 53.80 % and 61.14 % MC-LR, respectively; while PAA and PBS removed almost 100 % and 93.72 % MC-LR after 1 h adsorption, respectively (Table S3). With increase of adsorption time, MC-LR adsorption reached the adsorption equilibrium at various time (Fig. 2). BBA and BAW reached equilibrium at 40 h with maximal MC-LR removal of 49.11 % and 40.46 %, respectively. CAA and CAW were saturated at 48 h and removed 76.12 % and 96.22 % MC-LR, respectively. OAW and OBS reached equilibrium much quickly in 13 h and 7 h with maximum MC-LR removal of 48.52 % and 53.16 %, respectively (Table S3). Both PAA and PBS removed 100.00 % of MC-LR within 1 h and 3 h, respectively. When the initial MC-LR concentration increased to 30.0 mg/L, PAA adsorbed 99.90 % MC-LR after 10 h (Fig. 2g). PBS adsorbed 41.17 % of the initially seeded MC-LR at 15.0 mg/L after 48 h (Fig. 2h).

The adsorption of MC-LR by the eight adsorbents all followed pseudo second order kinetics (Fig. 3a). The calculated equilibrium adsorption capacity (q_e) of PAA were 75.09 mg/g, which was 4.81, 6.96 and 8.75 times higher than that of PBS (15.61 mg/g), CAW (10.79 mg/g), CAA (8.58 mg/g), respectively. The q_e of bamboo and oakwood-based adsorbents were the lowest, ranging from 4.57 mg/g (BAW) to 5.59 mg/g

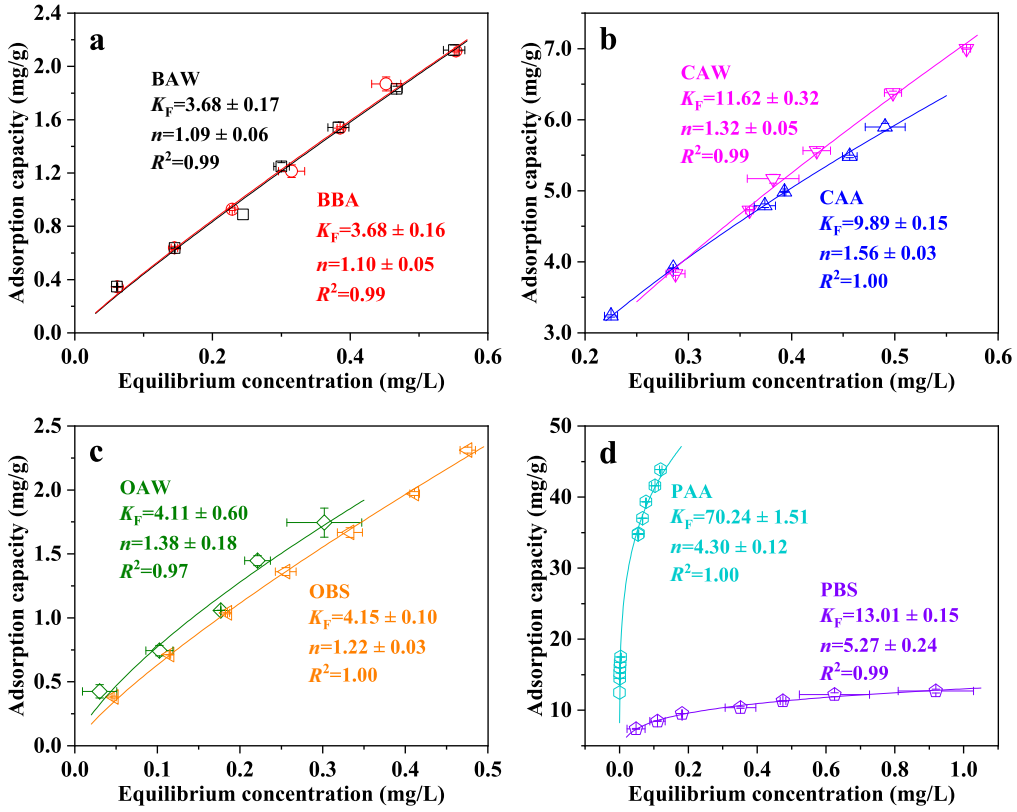

Fig. 1. MC-LR adsorption isotherms and Freundlich model fitting results of eight carbonaceous adsorbents. (a) BAW and BBA; (b) CAW and CAA; (c) OAW and OBS; (d) PAA and PBS. Experimental data are presented as colored data points, and the corresponding-colored lines are model fit.

(BBA). The observed rate constant (k_2) of OAW (0.27 mg/g/h) was the highest, followed by OBS (0.26 mg/g/h), PAA (0.26 mg/g/h) and BAW (0.22 mg/g/h). Accordingly, PAA exhibited the best adsorption performance towards MC-LR with the highest adsorption capacity and the second-highest adsorption rate. Although PBS had the second-highest adsorption capacity towards MC-LR, its observed rate constant was only half of PAA. Coconut shell-based adsorbents had higher adsorption capacity than bamboo and oakwood-based adsorbents, however, their observed rate constants were the lowest.

Coupling carbonaceous adsorbents with *Sphingopyxis* sp. m6 biodegradation successfully broke the threshold of MC-LR removal capacity by pure physiochemical adsorption. As shown in Fig. 2, MC-LR was continuously removed by coupled adsorption-biodegradation with the increase of reaction time for all adsorbents except for PAA. At the end of 48 h, most coupled adsorption-biodegradation reactions removed >90 % of initially seeded MC-LR at 4.5 mg/L. BAW coupled with *Sphingopyxis* sp. m6 had the lowest removal rate of 84.66 % (Table S3). Moreover, the coupled adsorption-biodegradation treatments all achieved much better MC-LR removal performance (Table S3) than pure *Sphingopyxis* sp. m6 treatment (33.66 %) (Fig. S1) after 13 h of reaction except for PAA and PBS, which consist with our previous work (Zhang et al., 2023). The MC-LR removal increased to 94.44 % in PBS + sp. m6 coupled treatment at the initial MC-LR concentration of 15 mg/L (Fig. 2h). However, the enhancement of the MC-LR removal for PAA coupled with *Sphingopyxis* sp. m6 was not observed since PAA adsorption alone rapidly removed nearly 100 % MC-LR within 10 h at the initial concentration of 30 mg/L. The coupled effect may be observed with much higher initial concentration of MC-LR.

The coupled adsorption-biodegradation treatment well-fitted to pseudo second order kinetics of adsorption at the first phase of reaction (0 to 13 h) (Fig. 3b), indicating carbon adsorption played the most important role in MC-LR removal during this period. Moreover, the coupled adsorption-biodegradation reaction improved MC-LR adsorption capacity (as indicated by sp. m6-q_e) for most (Fig. 3b) by comparing with the pure adsorption treatments at same reaction period (0 to 13 h) (Fig. S2). It suggests the positive contribution of biological removal of MC-LR by *Sphingopyxis* sp. m6. Namely, *Sphingopyxis* sp. m6 promoted the regeneration of carbonaceous adsorbents through: (i) direct degradation of MC-LR adsorbed on the surfaces of carbonaceous adsorbents, which simultaneously boost MC-LR's desorption and accelerate the re-exposure of active sites for more MC-LR adsorption, (ii) degradation of desorbed MC-LR that released from the inner pores of carbonaceous adsorbents that are not previously accessible by *Sphingopyxis* sp. m6 and their exoenzymes (size restriction to penetrate the mesopores of porous structure) (Salvador et al., 2015). However, the rate constants (sp. m6-k_2) of MC-LR removal decreased in the coupled adsorption-biodegradation reactions (Figs. 3b and S2). This is likely due to the attachment of *Sphingopyxis* sp. m6 onto adsorbents surfaces consequently blocked some corresponding active sites for MC-LR adsorption, which have been revealed by our recent published SEM images (Zhang et al., 2023). Although the attached *Sphingopyxis* sp. m6 actively removed MC-LR through biodegradation, biological removal rate of MC-LR still was slower than pure physiochemical adsorption. As a result, the sp. m6-k_2 was decreased in presence of *Sphingopyxis* sp. m6 during this phase.

From 18 h to 48 h, the MC-LR removal by the coupled adsorption-biodegradation well-fitted to first order kinetics of biodegradation in seven of eight treatments (Fig. 3c). Clearly, biological removal of MC-LR by *Sphingopyxis* sp. m6 played a key role in MC-LR removal after the physiochemical adsorption of MC-LR by carbonaceous adsorbents approached an equilibrium state. Furthermore, the coupled adsorption-biodegradation treatments increased the MC-LR biodegradation rates (Fig. 3c) for most by comparing with the pure biodegradation treatment (Fig. S1). It indicated that the carbonaceous adsorbents were conducive to the biodegradation of MC-LR.

To further validate the biological activity attached to carbonaceous

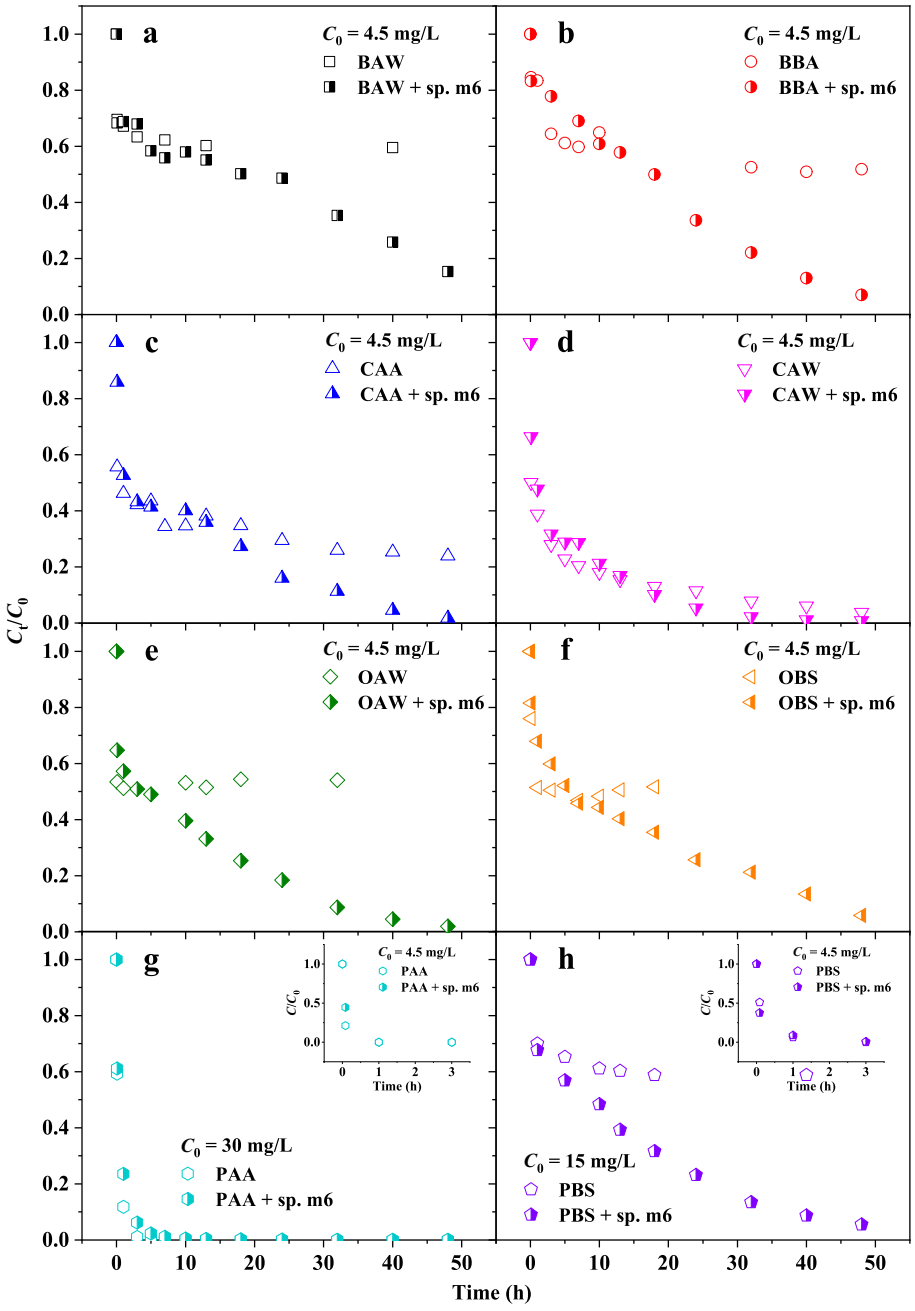

Fig. 2. Removal kinetics of MC-LR by pure adsorption treatments, and coupled adsorption-biodegradation treatments: (a) BAW; (b) BBA; (c) CAA; (d) CAW; (e) OAW; (f) OBS; (g) PAA; (h) PBS. (C_0 is the initial MC-LR concentration; C_t is the MC-LR concentration.)

adsorbents, we compared the viable *Sphingopyxis* sp. m6 counts over time during MC-LR removal experiments. In the absence of the carbonaceous adsorbents, the total number of viable *Sphingopyxis* sp. m6 declined with the increase of incubation time from 8.81 $\log_{10}$CFU/mL (0 h) to 6.23 $\log_{10}$CFU/mL (32 h) (Fig. S3). In comparison, the total numbers of viable *Sphingopyxis* sp. m6 coupled with carbonaceous adsorbents were significantly higher than that of pure *Sphingopyxis* sp. m6 test (Fig. S3), as indicated by the C_t/C_0 in Fig. 4. This result showed that the carbonaceous adsorbents were beneficial to the growth of *Sphingopyxis* sp. m6. Moreover, eight adsorbents exhibited varying degrees of beneficial effect on *Sphingopyxis* sp. m6 growth (Fig. 4). Pinewood-based adsorbents seemed to be the most supportive of *Sphingopyxis* sp. m6 (PAA and PBS), followed by coconut shell-based adsorbents (CAA and CAW).

Overall, the coupled adsorption-biodegradation treatments successfully achieved much better MC-LR removal performance than both pure adsorption and pure biodegradation treatments. Pinewood-based adsorbents (PAA and PBS) achieved the best performance in not only MC-LR physiochemical adsorption but also promoting *Sphingopyxis* sp. m6 growth; and coconut shell-based adsorbents (CAA and CAW) took the second place.

3.2. Properties of carbonaceous adsorbents

The physical and chemical properties of adsorbents were examined to understand the mechanisms of experimental observations. The specific surface areas (S_{BET}) of coconut shell and pinewood-based adsorbents were significantly higher than bamboo and oakwood-based adsorbents. S_{BET} of CAW was the highest (2304.00 m^2/g), followed by PAA (1749.30 m^2/g). The mean pore width (W) of adsorbents ranged

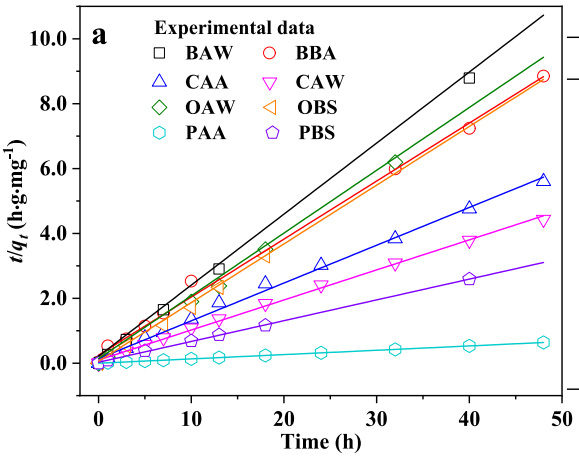

Pseudo second order model fitting parameters

Samples	q_e (mg/g)	k_2 (mg/g/h)	R^2
BAW	4.57 ± 0.12	0.22 ± 0.10	1.00
BBA	5.59 ± 0.13	0.13 ± 0.05	1.00
CAA	8.58 ± 0.17	0.10 ± 0.04	1.00
CAW	10.79 ± 0.15	0.09 ± 0.03	1.00
OAW	5.17 ± 0.19	0.27 ± 0.22	0.99
OBS	5.52 ± 0.30	0.26 ± 0.21	0.98
PAA	75.09 ± 0.05	0.26 ± 0.08	1.00
PBS	15.61 ± 0.17	0.13 ± 0.06	1.00

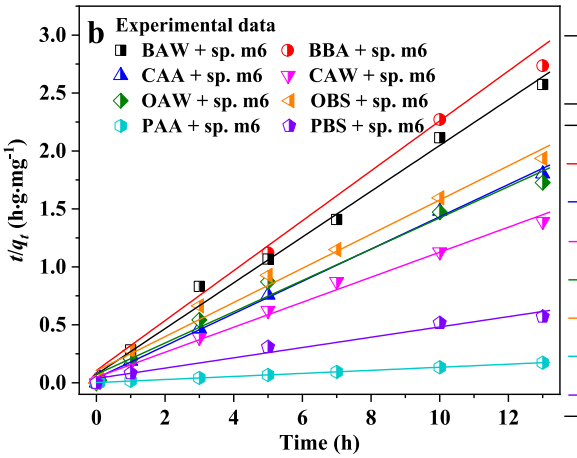

Pseudo second order model fitting parameters

Samples	sp. m6-q_e (mg/g)	sp. m6-k_2 (mg/g/h)	R^2
BAW + sp. m6	5.06 ± 0.18	0.54 ± 0.38	0.99
BBA + sp. m6	4.64 ± 0.22	0.43 ± 0.32	0.99
CAA + sp. m6	7.18 ± 0.15	0.48 ± 0.25	1.00
CAW + sp. m6	9.27 ± 0.32	0.24 ± 0.14	0.99
OAW + sp. m6	7.41 ± 0.40	0.25 ± 0.18	0.99
OBS + sp. m6	6.78 ± 0.32	0.21 ± 0.11	0.99
PAA + sp. m6	75.62 ± 0.58	0.08 ± 0.03	1.00
PBS + sp. m6	22.50 ± 2.19	0.05 ± 0.05	0.97

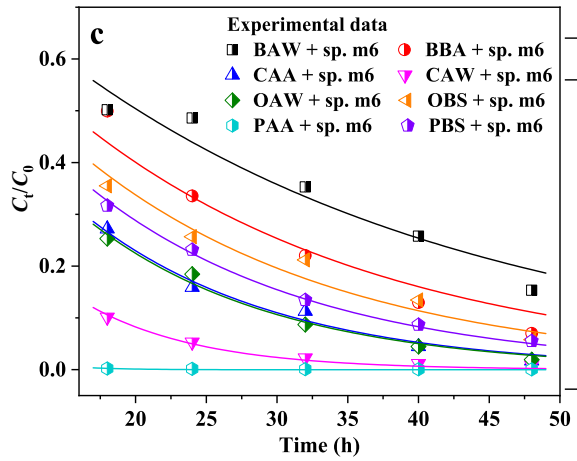

First order model fitting parameters

Samples	sp. m6-k_1 (h^{-1})	R^2
BAW + sp. m6	0.03 ± 0.002	0.94
BBA + sp. m6	0.05 ± 0.003	0.95
CAA + sp. m6	0.07 ± 0.002	0.98
CAW + sp. m6	0.12 ± 0.002	0.98
OAW + sp. m6	0.07 ± 0.002	0.99
OBS + sp. m6	0.05 ± 0.002	0.95
PAA + sp. m6	0.33 ± 0.022	-1.31
PBS + sp. m6	0.06 ± 0.001	1.00

Fig. 3. Pseudo-second order model fitting results of MC-LR removal kinetics in 0–48 h of pure adsorption tests (a), and 0–13 h of coupled tests (b); first order model fitting results of MC-LR removal kinetics of coupled tests from 18 to 48 h (c).

from 1.66 nm (CAW) to 6.68 nm (OAW) (Table 2). Total pore volume (PV_{total}) of bamboo and oakwood-based adsorbents were both lower than 0.1 cm^3/g, which were lower than corresponding coconut shell and pinewood-based adsorbents. As indicated by the lowest mean pore width (W = 1.66 nm), CAW was dominated by micropores (PV_{micro} = 92.39 % of PV_{total}), while mesopore volume only accounted for 0.02 cm^3/g. In the contrast, mesopore volume (PV_{meso}) of PAA was the highest (0.80 cm^3/g), which was 16 times of PBS (0.05 cm^3/g), 20 times of CAA (0.04 cm^3/g), 40 times of BBA, CAW, OBS (0.02 cm^3/g), and 80 times of BAW, OAW (0.01 cm^3/g) (Table 2). Since mesopore has been reported as an important positive contributor to adsorption capacity towards MC-LR (Li et al., 2018; Park et al., 2018; Teng et al., 2015), with the highest PV_{meso}, PAA exhibited the best adsorption capacity towards MC-LR (Figs. 1, 2 and 3a). Despite the highest S_{BET}, the adsorption capacity of CAW towards MC-LR was limited by its low PV_{meso}. Moreover, the higher available surface area (i.e., accessible external and internal surface area) of adsorbents would contribute to the attachment and the growth *Sphingopyxis* sp. m6 in coupled adsorption-biodegradation tests (Mohanty et al., 2014). The favorable conditions were evident in the higher viable *Sphingopyxis* sp. m6 counts (sp. m6–32) after coculturing with coconut shell and pinewood-based adsorbents (Figs. 4 and S3). Nevertheless, the bacterial count of *Sphingopyxis* sp. m6 at 32 h was

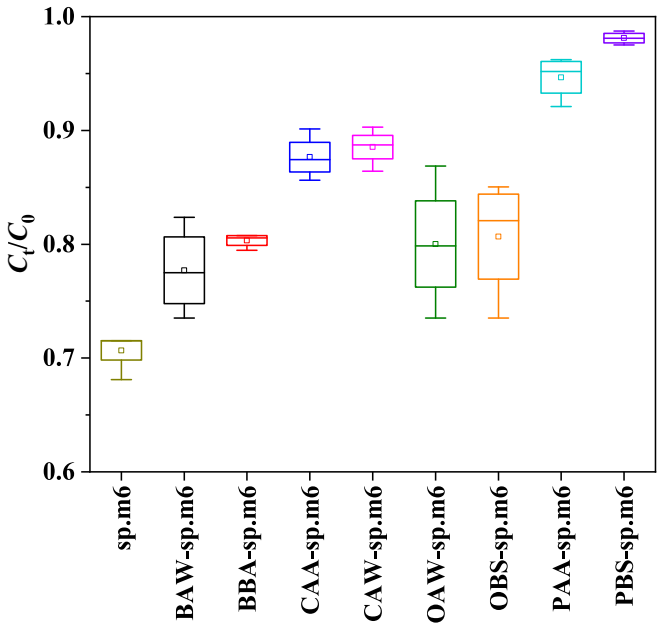

Fig. 4. *Sphingopyxis* sp. m6 viable counts after incubating without or with pure carbonaceous adsorbents in M9 media. C_0 is the average initial total number of viable *Sphingopyxis* sp. m6 at 0 h (C_0 = [sp. m6]$_0$ = 8.81 $\log_{10}$CFU/mL); C_t is total number of viable *Sphingopyxis* sp. m6 at 32 h.

higher on pinewood-based adsorbents than that on coconut shell-based adsorbents. It suggested that S_{BET} was not the most accurate index reflecting the actual surface area for bacterial attachment because S_{BET} included the internal surface area of micro/mesopores within adsorbents that may be inaccessible to *Sphingopyxis* sp. m6 (Mohanty et al., 2014).

The ash content of the eight adsorbents ranged from 1.43 % (OAW) to 7.70 % (PAA) (Table 3). The ash content exhibited a significant positive correlation with PV_{meso} ($r = 0.79$, $p \leq 0.001$, Fig. S5), which was consist with previous studies (Li et al., 2018). PAA, with the highest ash content, is conducive to provide nutrients for the growth of *Sphingopyxis* sp. m6 during the coupled adsorption and biodegradation tests (Gomez et al., 2014).

There was no obvious difference in atomic ratios of H/C (0.03–0.04) among the adsorbents except for PAA (0.06) (Table 3), indicating that PAA contained lower aromatic structures (Li et al., 2018). It has been reported that aromatic structures of carbonaceous adsorbents could enhance the π-π electron donor-acceptor interaction between the adsorbents and MC-LR during adsorption process by providing larger π-electron-rich moieties to act as more π-donors, and thus improve MC-LR adsorption capability (Frišták et al., 2020; Li et al., 2018; Song et al., 2021). However, the relatively lower aromaticity in PAA did not impact its MC-LR adsorption performance, suggesting that π-π electron donor-acceptor interaction was not the major driving force for MC-LR adsorption in this study. For the bamboo and oakwood adsorbents, the atomic ratios of O/C and (N + O)/C of activated carbon were both lower than that of biochar, implying higher pyrolysis temperature promoted the removal of polar functional groups of organic matter (Hassan et al., 2020; Weber and Quicker, 2018). However, the O/C and (N + O)/C values of PAA was about two times higher than PBS, confirming high mineral ash content could protect the polar functional groups of organic matter from being removed during pyrolysis process (Li et al., 2018). Higher values of O/C and (N + O)/C indicated the greater polarity of carbonaceous adsorbents, which can facilitate MC-LR adsorption through forming more hydrogen bonds between the O- and H-containing polar groups on the adsorbents and H, N and O atoms of MC-LR molecules (Li et al., 2018; Park et al., 2020; Zhang et al., 2023; Zhao and Li, 2022). Hence, the highest O/C and (N + O)/C of PAA helped to explain its best adsorption performance towards MC-LR.

The total surface functional groups of PAA (1.77 mmol/g) were the highest, followed by PBS (1.46 mmol/g), and OBS (1.15 mmol/g) (Fig. 5a). Acidic functional groups were dominant on PAA (1.68 mmol/g accounted for >90 % of total), but were not detected on PBS and CAW (< 0.0125 mmol/g) (Fig. 5a). The carboxylic, phenolic, lactonic functional groups accounted for 47.87 %, 32.94 %, 19.19 %, respectively, of PAA's acidic functional groups (Fig. 5b). The hydrogen bonds between carboxylic groups and MC-LR molecules further boosted the PAA adsorption of MC-LR. Moreover, functional groups in carbonaceous adsorbents, especially surface O-containing groups, would also be beneficial for electron transfer between microorganisms, and

Table 2
Surface and pore properties of tested carbonaceous adsorbents.

Carbon adsorbents	W (nm)	S_{BET} (m^2/g)	S_{micro} (m^2/g)	S_{meso} (m^2/g)	PV_{total} (cm^3/g)	PV_{micr} (cm^3/g)	PV_{meso} (cm^3/g)
BAW	5.67	10.08	3.02	2.45	0.02	0.00	0.01
BBA	2.45	118.19	62.90	7.30	0.07	0.04	0.02
CAA	2.00	479.71	338.74	15.01	0.24	0.17	0.04
CAW	1.66	2304.00	1576.10	15.60	0.92	0.85	0.02
OAW	6.68	6.62	3.32	1.08	0.02	0.00	0.01
OBS	4.42	32.60	10.96	7.81	0.04	0.01	0.02
PAA	3.40	1749.30	913.45	207.05	1.47	0.55	0.80
PBS	2.09	430.03	306.06	19.36	0.22	0.15	0.05

Note: micropore is defined as pore size ≤2.0 nm, mesopore has pore size between 2 nm to 50 nm (Li et al., 2018).

Table 3
Ash content, elemental composition and atomic ratio of tested carbonaceous adsorbents.

Carbon adsorbents	Ash (wt%)	Elemental composition (wt%)				Atomic ratio		
		C	H	N	O	H/C	O/C	(N + O)/C
BAW	2.82 ± 0.17	79.22 ± 0.13	3.18 ± 0.08	0.90 ± 0.06	13.88 ± 0.21	0.04 ± 0.00	0.18 ± 0.00	0.19 ± 0.00
BBA	3.42 ± 0.28	70.77 ± 0.44	3.11 ± 0.05	1.12 ± 0.01	21.58 ± 0.08	0.04 ± 0.00	0.30 ± 0.00	0.32 ± 0.00
CAA	4.58 ± 0.16	80.53 ± 0.14	2.68 ± 0.10	0.76 ± 0.01	11.45 ± 0.24	0.03 ± 0.00	0.14 ± 0.00	0.15 ± 0.00
CAW	1.82 ± 0.05	78.48 ± 0.01	2.68 ± 0.00	0.36 ± 0.03	16.67 ± 0.05	0.03 ± 0.00	0.21 ± 0.00	0.22 ± 0.00
OAW	1.43 ± 0.36	86.28 ± 0.30	2.32 ± 0.30	0.59 ± 0.02	9.39 ± 0.37	0.03 ± 0.00	0.11 ± 0.00	0.12 ± 0.00
OBS	4.07 ± 0.49	78.86 ± 0.25	3.15 ± 0.04	0.49 ± 0.03	13.44 ± 0.67	0.04 ± 0.00	0.17 ± 0.01	0.18 ± 0.01
PAA	7.70 ± 0.92	60.10 ± 0.71	3.68 ± 0.05	0.53 ± 0.01	28.00 ± 1.04	0.06 ± 0.00	0.47 ± 0.02	0.47 ± 0.02
PBS	4.22 ± 0.02	75.61 ± 0.19	2.49 ± 0.07	0.64 ± 0.02	17.05 ± 0.22	0.03 ± 0.00	0.23 ± 0.00	0.23 ± 0.00

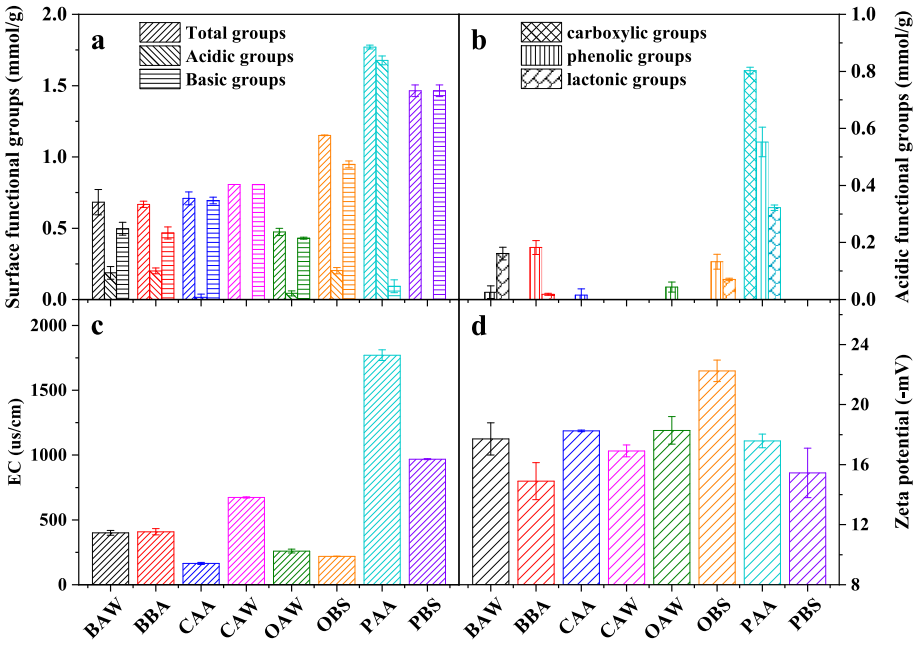

Fig. 5. Properties of tested carbonaceous adsorbents. (a) Surface functional groups; (b) types of acidic functional groups; (c) electrical conductivity; (d) zeta potential in M9 mineral media.

consequently increased the biodegradation rate of contaminants (Ren et al., 2020; Wang et al., 2020). Obviously, the highest total functional groups, especially carboxylic groups, are not only positively contribute to the super MC-LR adsorption performance of PAA but also are advantageous to the growth of *Sphingopyxis* sp. m6. However, the carboxylic functional groups were all below the detection limit (< 0.0125 mmol/g) for all other tested adsorbents (Fig. 5b). In the absence of detectable acidic groups, PBS, with the second highest content of total functional groups, achieved the second-best MC-LR adsorption performance. This result implied that hydrogen bonds derived from acidic functional groups were not the major driving force for MC-LR adsorption by PBS.

PAA had the highest EC value (1770.44 μs/cm) followed by PBS (968.78 μs/cm), and CAW (673.44 μs/cm) (Fig. 5c). The high EC of PAA not only is beneficial for MC-LR adsorption but also enhances MC-LR biodegradation because of the following reasons. i) High EC indicated high number of soluble salts in adsorbents, which increase the amount of cation-π bonds for MC-LR adsorption (Gai et al., 2014). ii) High soluble salts provide nutrients for the growth of *Sphingopyxis* sp. m6, and consequently enhance the biological removal of MC-LR in coupled adsorption and biodegradation treatments. iii) Carbonaceous adsorbents can function as an electron shuttle to facilitate the electron transfer from microorganisms to contaminants (Ren et al., 2023; Yu et al., 2015). As a result, the microbial transformation rate of organic contaminants is promoted (Gao et al., 2023; Tong et al., 2014).

The pH of tested carbonaceous adsorbents in ultrapure water were mostly basic, ranging from 8.89 (OBS) to 10.60 (CAW) except for PAA (pH = 2.23) (Fig. S4). However, the pH of all carbonaceous adsorbents in M9 media were all the same and kept stable at neutral pH (Fig. S4) due to the buffer effect of M9 media (Table S1). The neutral pH is the most favorable conditions for *Sphingopyxis* sp. m6 growth and biodegradation of MC-LR (Ding et al., 2018). All tested adsorbents were negatively charged in M9 media (pH = 7.0) (Fig. 5d). The zeta potential ranged from −14.90 mV (BBA) to −22.25 mV (OBS). Since MC-LR molecules are also negatively charged at neutral pH (Song et al., 2021; Zhao and Li, 2022), an electrostatic repulsion between MC-LR and adsorbents is expected. However, the experimental results of this study indicated that electrostatic repulsions did not play an important role to hinder the MC-LR adsorption, likely due to its weak effect in comparison with other factors (i.e. mesopore filling) that strongly favor the adsorption. Coupling *Sphingopyxis* sp. m6 with adsorbents neutralized the negative zeta potentials in some degree since *Sphingopyxis* sp. m6 was positively charged in M9 media. Yet, the adsorption rate was not enhanced in the coupled adsorption-biodegradation reactions, further confirmed the minor role of electrostatic repulsions. In fact, the adsorption rate of MC-LR actually decreased (Figs. 3b and S2) because the attachment of *Sphingopyxis* sp. m6 onto adsorbents surfaces inactivated some corresponding active sites for MC-LR adsorption (Zhang et al., 2023).

Overall, properties of adsorbents greatly influenced MC-LR removal performance in both pure adsorption treatments and coupled adsorption and biodegradation treatments. Pinewood-based adsorbents (PAA and PBS) showed the super performance is not only because of their MC-LR adsorption capacity but also because of their support in *Sphingopyxis* sp. m6 growth and MC-LR biodegradation due to their high mesopore volume, functional groups and electric conductivity.

3.3. Key factors for MC-LR removal

Despite previous studies reporting the effect of adsorbents properties on MC-LR removal, their quantitative mechanisms remain unclear. To identify the deterministic factors for MC-LR removal, spearman correlation coefficients between adsorbents' properties and their corresponding MC-LR removal performance were presented in a heat map (Fig. 6). VPA, shown in Fig. 7, quantified the specific contributions of key factors to the MC-LR removal performance to elucidate mechanisms of MC-LR removal by the coupled process.

3.3.1. Pure adsorption

3.3.1.1. Adsorption capacity (q_e). In the adsorbents only tests, pore parameters (i.e., PV_{total}, PV_{micro}, PV_{meso}, S_{BET}, S_{micro}, S_{meso}), surface functional groups (i.e., total groups, carboxylic groups), polarity (i.e., O/C, (N + O)/C) and other parameters (i.e., EC, ash) were all significantly positively correlated ($p \leq 0.01$) with the MC-LR adsorption capacity related parameters (i.e., K_F, q_e) (Fig. 6). S_{meso} had the strongest correlation with q_e ($r = 0.95$), followed by PV_{meso} ($r = 0.93$). These results statistically confirmed that pore related parameters, especially

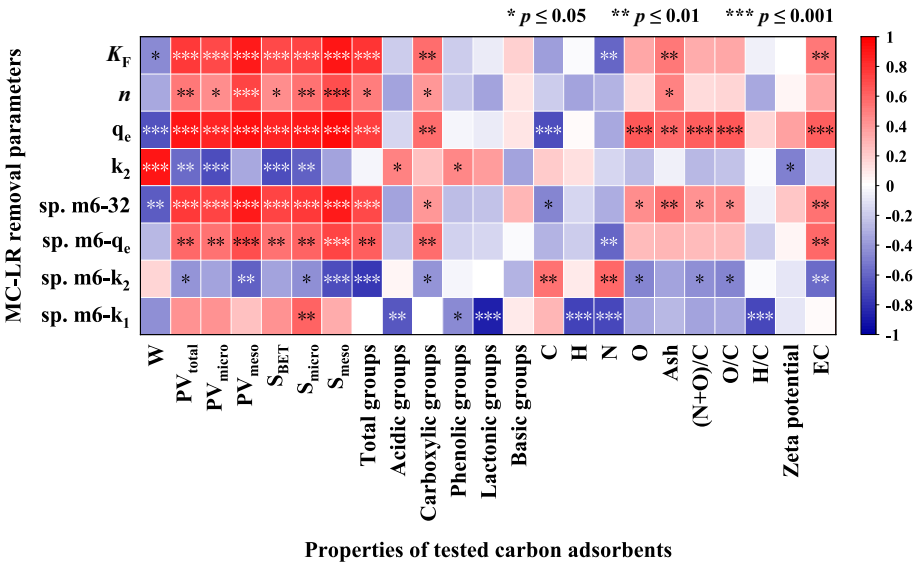

Fig. 6. Heat map of the correlations between the adsorbents' properties and MC-LR removal performance. On the y-axis, top four parameters are results of absorbents only tests, the next four are results for coupled absorbent-*Sphingopyxis* sp. m6 tests. sp.m6-32 is the total viable *Sphingopyxis* sp. m6 bacteria counted at 32 h.

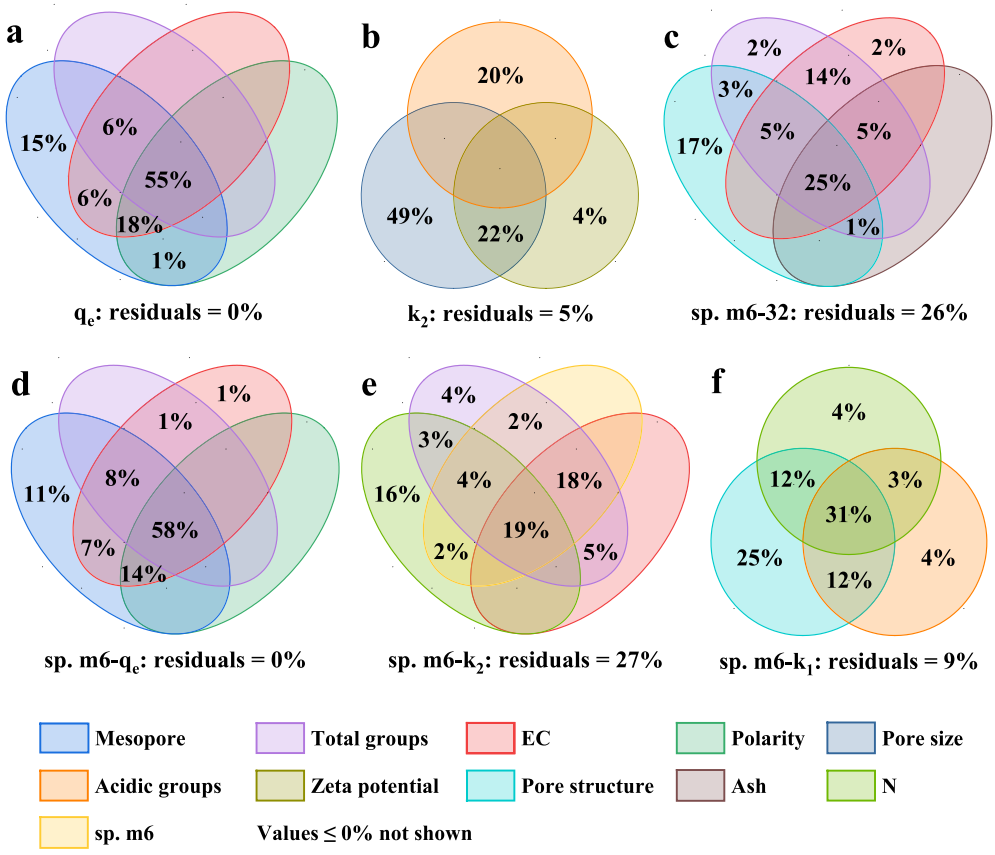

Fig. 7. Quantitative contribution of adsorbents properties to MC-LR removal performance according to the VPA. MC-LR adsorption capacity (a) and rate (b) in pure adsorbents' tests; *Sphingopyxis* sp. m6 growth in coupled tests (c); MC-LR adsorption capacity (d) and rate (e) before 13 h of coupled tests; MC-LR biological removal rate (f) after 13 h of coupled tests.

mesopores, were the most important positive contributors to MC-LR adsorption capacity (Park et al., 2018; Teng et al., 2013a, 2015).

VPA calculations further revealed that mesopores (e.g., S_{meso}), functional groups (e.g., total groups), polarity (e.g., O/C), and EC altogether contributed to 100 % of total variance of adsorption capacity (e.g., q_e) (Fig. 7a). Specifically, the mesopores singly contributed to 15 % of the total variation of adsorption capacity, confirming MC-LR mainly adsorbed by carbonaceous adsorbents through mesopore filling (Li et al., 2018; Zhao and Li, 2022). MC-LR is a three-dimensional macromolecule with the maximum length and second-widest dimension of 2.94 nm and 2.55 nm, respectively (Teng et al., 2013b; Zhang et al., 2011; Zhao and Li, 2022). Thus, MC-LR sorption via pore-filling can only occupy

mesopores (2–50 nm width) and larger-size pores but cannot access micropores (≤ 2 nm width) (Li et al., 2018; Teng et al., 2013b; Zhao and Li, 2022). The joint effects of mesopores with EC, polarity and total functional groups contributed to 85 % of the variation. However, none of EC, polarity and total functional groups had important individual contributions to the total variation of the adsorption capacity. Accordingly, they affected adsorption capacity mainly through their synergistic effects with mesopores (Fig. 7a). The joint effect of EC with mesopores (6 %) had higher contribution than the joint effect of polarity with mesopores (1 %) or the joint effect of total functional groups with mesopores (0 %). These above results indicated that cations in mesopores positively promoted MC-LR adsorption within mesopores, which was likely driven by the cation-π interactions (Y. Liu et al., 2021). Meanwhile, polar groups (H- and O-containing groups, e.g., carboxyl groups and phenolic groups) also played a beneficial role in capturing MC-LR within mesopores by π-π bonds and/or hydrogen bonds (Li et al., 2018; Park et al., 2020; Zhang et al., 2023; Zhao and Li, 2022). The sites on mesopores surfaces containing cations and polar groups were the favorable adsorption sites for MC-LR, contributing to 18 % of the variation of adsorption capacity (Fig. 7a). Furthermore, the joint effect of these factors explained 55 % of the variation of adsorption capacity. In general, mesopores alone can adsorb MC-LR through mesopore filling, meanwhile, EC, polarity and functional groups of adsorbents can enhance the utilization of mesopores to enhance the adsorption capacity towards MC-LR. However, the maximum adsorption capacity was largely determined by the available mesopores. The highly significant positive correlations between PV_{meso} and adsorption affinity (i.e., n) of adsorbents towards MC-LR ($r = 0.74$, $p \leq 0.001$) confirmed the important role of mesopores in controlling the MC-LR adsorption. Therefore, VPA results further confirmed that PAA had the best MC-LR adsorption capacity because of its highest mesopore volumes, highest EC and polar groups.

3.3.1.2. Adsorption rate (k_2). MC-LR molecules can easily access mesopores with larger size due to the decrease of pore filling resistance with the increase of pore width (Zhao and Li, 2022). MC-LR adsorption rate increased with the increase of mesopore width, which was revealed by the highest significant positive correlation between adsorbents' mean pore width (W) and MC-LR adsorption rate constant (i.e., k_2) ($r = 0.90$, $p \leq 0.001$) (Fig. 6). However, materials with larger pore width typically have lower pore volumes and specific surface area. Therefore, both pore volume (PV_{total}, PV_{micro}, PV_{meso}) and specific surface area (S_{BET}, S_{micro}, S_{meso}) were negatively correlated with adsorption rate constant (Fig. S5). The acidic groups (e.g., phenolic and lactonic groups) were positively correlated with the adsorption rate, while zeta potential of the adsorbents showed negative correlation with adsorption rate (Fig. 6).

According to the VPA results (Fig. 7b), pore size (W), surface charge (e.g., zeta potential) and acidic groups altogether could account for 95 % of total variance of MC-LR adsorption rate (e.g., k_2). Wherein, pore size played the most important role in determining adsorption rate with 49 % of individual contribution to total variance of k_2 (Fig. 7b). The single contribution of surface charges to the total variance was the lowest (4 %), confirming electrostatic repulsion was not a major driving force hindering MC-LR adsorption onto carbonaceous adsorbents. The joint effect of surface charge with pore size (22 %) was much higher, implying the effect of surface charges on adsorption rate mainly depending on pore size. In contract to surface charges, there was almost no joint effect of acidic groups with pore size on adsorption rate. While the acidic groups singly explained 20 % of the total variance, indicating acidic groups (e.g., lactonic, phenolic and carboxyl groups) affected adsorption rate through surface adsorption rather than mesopore filling.

Therefore, OAW achieved the highest adsorption rate towards MC-LR owing to its largest mean pore width. With the highest content of acidic groups, PAA had the second highest adsorption rate although its mean pore width was lower than OBS and BAW.

3.3.2. Coupled adsorption and biodegradation

3.3.2.1. Growth of Sphingopyxis sp. m6 (sp. m6-32). In the coupled adsorption and biodegradation tests, the total viable *Sphingopyxis* sp. m6 (sp. m6–32) ($p \leq 0.01$) were significantly positively correlated with pore parameters (PV_{total}, PV_{micro}, PV_{meso}, S_{BET}, S_{micro}, S_{meso}), the total functional groups, ash and EC (Fig. 6). Wherein, pore structure (i.e., W, PV_{total}), total groups, EC and ash could explain 74 % of the total variance of sp. m6–32 altogether (Fig. 7c). Single contribution by pore structure was much higher than single effects by other factors, moreover, pore structure attributed to 51 % of the total variation of sp. m6–32, synergistically with total groups, EC and ash of the absorbent. It revealed the crucial role of pore structure in promoting the attachment of *Sphingopyxis* sp. m6 onto carbonaceous adsorbents and encouraging the survival and proliferation of *Sphingopyxis* sp. m6. Total functional groups, EC and ash all had very limited individual contribution to sp. m6–32 (≤ 2 %), further suggesting that these factors contributed to the growth of *Sphingopyxis* sp. m6 through their joint effects with pore structure rather than single effects. The residual of total variance of sp. m6–32 could be explained by the variances of adsorbent's MC-LR physiochemical adsorption capability (i.e., K_F and n), as indicated by their significantly positive correlations ($p \leq 0.001$) with sp. m6–32 (K_F: $r = 0.87$, n: $r = 0.84$) (Fig. S5). However, the adsorption capability was not used as a direct explanatory variable together with other factors because of the strong collinearity.

3.3.2.2. Adsorption capacity at the first period (sp. m6-q_e). During the first phase of coupled adsorption-biodegradation tests (0−13 *h*), the correlations between the properties of adsorbents and their adsorption capacity (sp. m6-q_e) towards MC-LR were similar to those in pure adsorption tests (Fig. 7d). According to VPA results, the single contribution of mesopores to adsorption capacity was much higher than the single contributions of total functional groups, EC and polarity, although it decreased from 15 % in the pure adsorption tests to 11 % in the coupled adsorption-biodegradation tests. The joint effects of mesopores with total functional groups, EC and polarity still contributed to 87 % of the variation. The results indicated that the adsorbents' properties, especially mesopores rich in cations, and/or had polarity and/or functional groups (e.g., carboxylic groups), still played the most important positive role in determining their MC-LR adsorption capacity at the first period (0–13 h).

3.3.2.3. Adsorption rate at the first period (sp. m6-k_2). Addition of *Sphingopyxis* sp. m6 changed the key contributors to the adsorption rate. In comparison with pure adsorption treatments, pore size no longer played a key role in determining adsorption rate constant (i.e., sp. m6-k_2) during the first 13 h reaction of coupled treatments. Elements (e.g., N), total functional groups, viable *Sphingopyxis* sp. m6 counts (sp. m6–32) and EC explained 73 % of the total variance of sp. m6-k_2 altogether (Fig. 7e). Wherein, sp. m6–32 ($r = -0.70$, $p \leq 0.001$) exhibited a significant negative correlation with sp. m6-k_2 (Figs. 6 and S5), confirming that biodegradation was not the main driving forces for MC-LR removal in the early stage of coupled adsorption-biodegradation tests. *Sphingopyxis* sp. m6 growth and its joint effects with elements, total functional groups and EC accounted for 45 % of the total variance of sp. m6-k_2. sp. m6-k_2 of PAA and PBS were the lowest, which was likely due to the attachment of *Sphingopyxis* sp. m6 onto surfaces that blocking mesopores from rapid physiochemical adsorption of MC-LR (Salvador et al., 2015) (Fig. 3b). N positively related to sp. m6-k_2 (Fig. 6) probably because of its negative correlation with sp. m6–32 (Fig. S5). Meanwhile, total functional groups and EC were negatively related to sp. m6-k_2 due to their significantly positive correlations with sp. m6–32 (Fig. S5). Residual 27 % of sp. m6-k_2 variance could be explained by the variances of mesopores and acidic groups (especially carboxyl groups), which were the positive influencing factors for promoting the growth of

Sphingopyxis sp. m6 but the negative contributors to sp. m6-k_2. Overall, woody carbonaceous adsorbents could provide favorable conditions (e.g., offering accessible attaching sites, supplying nutrients and acting as electron shuttle) for the survival and proliferation *Sphingopyxis* sp. m6 during coupled tests. However, the proliferation of *Sphingopyxis* sp. m6 produced dual effect on MC-LR removal during the initial phase of the reaction in coupled tests, namely slightly enhanced the adsorption capacity of MC-LR but negatively impacted adsorption rate.

3.3.2.4. Biodegradation rate at the second period (sp. m6-k_1). At the second phase of the coupled adsorption and biodegradation tests (after 13 h of reaction), pore structure related parameters (especially pore volumes and specific surface areas) (Fig. 6), the total viable *Sphingopyxis* sp. m6 (sp. m6–32) (Fig. S5) and MC-LR adsorption capacity (sp.m6-q_e) (Fig. S5) were positively correlated to MC-LR biodegradation rate (i.e., sp.m6-k_1). In this period, S_{BET} singly explained 25 % of the total variance of sp. m6-k_1, which was more than six times higher than the individual contributions of element N (4 %) and acidic groups (4 %) (Fig. 7f). Once again, these quantitative results (Figs. 6 and S5) confirmed that adsorbent surface areas positively affect biodegradation removal of MC-LR through promoting the growth of *Sphingopyxis* sp. m6 and enhancing the capture of MC-LR. Referring to experimental data, CAW realized the highest sp. m6-k_1 likely because of the highest specific surface area.

As discussed above, adsorbents properties significantly affected both adsorption and biodegradation removal of MC-LR. VPA results further quantitatively revealed the most important positive role of pore structure on influencing MC-LR adsorption capability and the growth of *Sphingopyxis* sp. m6 and biodegradation of MC-LR.

4. Conclusions

In this study, mechanisms of the coupled physiochemical adsorption and biodegradation for MC-LR removal was investigated to provide insights for future engineering design of drinking water treatment for toxin removal. The key influencing factors and removal mechanism were quantitatively analyzed via VPA. The following conclusions can be drawn from the study:

1. For pure physiochemical adsorption, the mesopore was the most important positive contributor to adsorption capacity of MC-LR, which contributed 100 % to the total variation of adsorption capacity synergistically with EC, polarity and total functional groups. Mean pore size and acidic groups were the dominant favorable factors for adsorption rate with individual contributions of 49 % and 20 %.
2. At the first phase (0–13 h) of coupled adsorption-biodegradation, *Sphingopyxis* sp. m6 slightly enlarged the adsorption capacity of MC-LR with no significant change of dominant removal mechanism. However, a decrease of the adsorption rate was found, likely due to blocking critical adsorption sites by the attached bacteria on adsorbent surfaces.
3. Coupled adsorption and biodegradation broke the equilibrium threshold of pure physiochemical adsorption through biodegradation of MC-LR. Pore structure was the key factor benefiting the attachment and growth of *Sphingopyxis* sp. m6 and MC-LR biological removal rate, with corresponding related contributions of 51 % and 80 %, respectively.
4. Pinewood-based adsorbents not only exhibited the highest MC-LR adsorption capacity but also provided the most favorable conditions for MC-LR biological removal.

CRediT authorship contribution statement

Shengyin Tang: Writing – review & editing, Writing – original draft, Visualization, Project administration, Methodology, Investigation, Formal analysis, Data curation, Conceptualization. **Lixun Zhang:** Methodology, Investigation, Conceptualization. **Haoxin Zhu:** Methodology, Investigation. **Sunny C. Jiang:** Writing – review & editing, Writing – original draft, Supervision, Resources, Project administration, Funding acquisition, Conceptualization.

Declaration of competing interest

The authors declare that they have no known competing financial interests or personal relationships that could have appeared to influence the work reported in this paper.

Data availability

Data will be made available on request.

Acknowledgements

Financial support for this project was partially provided by the U. S. National Science Foundation (Award numbers 2128480 and 1806066), Shenzhen Science and Technology Program (WDZC20231128 115832002) and National Natural Science Foundation of China (52300209). The George E. Hewitt Foundation Postdoctoral Fellowship for Medical Research to Dr. Lixun Zhang is acknowledged. We also give special thanks to Dr. Zhiquan Song for his help in cultivating *Sphingopyxis* sp. m6, Dr. Felix Grun and UCI's Mass Spectrometry Facility for mass spectrometric analysis, and Dr. Dmitry A. Fishman and UCI Laser Spectroscopy Labs for surface charge analysis.

Appendix A. Supplementary data

Supplementary data to this article can be found online at https://doi.org/10.1016/j.scitotenv.2024.173370.

References

ASTM, 2021. Annual Book of ASTM Standards. Standard Test Method for Chemical Analysis of Wood Charcoal. ASTM D1762-84(2021). ASTM International, pp. 1–2.
Bardestani, R., Kaliaguine, S., 2018. Steam activation and mild air oxidation of vacuum pyrolysis biochar. Biomass Bioenergy 108, 101–112.
Dai, Y., Zhang, N., Xing, C., Cui, Q., Sun, Q., 2019. The adsorption, regeneration and engineering applications of biochar for removal organic pollutants: a review. Chemosphere 223, 12–27.
Ding, Q., Liu, K., Xu, K., Sun, R., Zhang, J., Yin, L., et al., 2018. Further understanding of degradation pathways of microcystin-LR by an indigenous Sphingopyxis sp. in environmentally relevant pollution concentrations. Toxins 10, 536.
Dutta, T., Kim, T., Vellingiri, K., Tsang, D.C.W., Shon, J.R., Kim, K.-H., et al., 2019. Recycling and regeneration of carbonaceous and porous materials through thermal or solvent treatment. Chem. Eng. J. 364, 514–529.
Foo, K.Y., Hameed, B.H., 2012. Microwave-assisted regeneration of activated carbon. Bioresour. Technol. 119, 234–240.
Frišták, V., Laughinghouse IV, H.D., Bell, S.M., 2020. The use of biochar and pyrolysed materials to improve water quality through microcystin sorption separation. Water 12, 2871.
Gai, X., Wang, H., Liu, J., Zhai, L., Liu, S., Ren, T., et al., 2014. Effects of feedstock and pyrolysis temperature on biochar adsorption of ammonium and nitrate. PLoS One 9, e113888.
Gao, Y., Sun, Y., Song, W., Jia, Y., Li, A., Wang, S., 2023. Intrinsic properties of biochar for electron transfer. Chem. Eng. J. 475, 146356.
Gomez, J., Denef, K., Stewart, C., Zheng, J., Cotrufo, M., 2014. Biochar addition rate influences soil microbial abundance and activity in temperate soils. Eur. J. Soil Sci. 65, 28–39.
Hassan, M., Liu, Y., Naidu, R., Parikh, S.J., Du, J., Qi, F., et al., 2020. Influences of feedstock sources and pyrolysis temperature on the properties of biochar and functionality as adsorbents: a meta-analysis. Sci. Total Environ. 744, 140714.
Huang, F., Gao, L.-Y., Wu, R.-R., Wang, H., Xiao, R.-B., 2020. Qualitative and quantitative characterization of adsorption mechanisms for Cd2+ by silicon-rich biochar. Sci. Total Environ. 731, 139163.
Initiative IB, 2015. IBI Biochar Standards. Standardized Product Definition and Product Testing Guidelines for Biochar That Is Used in Soil-Version 2.1, pp. 1–61.
Kano, F., Abe, I., Kamaya, H., Ueda, I., 2000. Fractal model for adsorption on activated carbon surfaces: Langmuir and Freundlich adsorption. Surf. Sci. 467, 131–138.
Li, J., Cao, L., Yuan, Y., Wang, R., Wen, Y., Man, J., 2018. Comparative study for microcystin-LR sorption onto biochars produced from various plant-and animal-

wastes at different pyrolysis temperatures: influencing mechanisms of biochar properties. Bioresour. Technol. 247, 794–803.
Li, Z., Chen, J., Wang, C., Zhao, J., Wei, Q., Ma, X., et al., 2023. Study on the removal and degradation mechanism of microcystin-LR by the UV/Fenton system. Sci. Total Environ. 892, 164665.
Liu, B.-L., Fu, M.-M., Xiang, L., Feng, N.-X., Zhao, H.-M., Li, Y.-W., et al., 2021a. Adsorption of microcystin contaminants by biochars derived from contrasting pyrolytic conditions: characteristics, affecting factors, and mechanisms. Sci. Total Environ. 763, 143028.
Liu, Y., Liu, S., Xu, C., Lin, M., Li, Y., Shen, C., et al., 2021b. Epitopes prediction for microcystin-LR by molecular docking. Ecotoxicol. Environ. Saf. 227, 112925.
Mohanty, S.K., Cantrell, K.B., Nelson, K.L., Boehm, A.B., 2014. Efficacy of biochar to remove Escherichia coli from stormwater under steady and intermittent flow. Water Res. 61, 288–296.
Nunes, K.G.P., Sfreddo, L.W., Rosset, M., Féris, L.A., 2021. Efficiency evaluation of thermal, ultrasound and solvent techniques in activated carbon regeneration. Environ. Technol. 42, 4189–4200.
Park, J.-A., Jung, S.-M., Yi, I.-G., Choi, J.-W., Kim, S.-B., Lee, S.-H., 2017a. Adsorption of microcystin-LR on mesoporous carbons and its potential use in drinking water source. Chemosphere 177, 15–23.
Park, J.-A., Yang, B., Park, C., Choi, J.-W., van Genuchten, C.M., Lee, S.-H., 2017b. Oxidation of microcystin-LR by the Fenton process: kinetics, degradation intermediates, water quality and toxicity assessment. Chem. Eng. J. 309, 339–348.
Park, J.-A., Jung, S.-M., Choi, J.-W., Kim, J.-H., Hong, S., Lee, S.-H., 2018. Mesoporous carbon for efficient removal of microcystin-LR in drinking water sources, Nak-Dong River, South Korea: application to a field-scale drinking water treatment plant. Chemosphere 193, 883–891.
Park, J.-A., Kang, J.-K., Jung, S.-M., Choi, J.-W., Lee, S.-H., Yargeau, V., et al., 2020. Investigating microcystin-LR adsorption mechanisms on mesoporous carbon, mesoporous silica, and their amino-functionalized form: surface chemistry, pore structures, and molecular characteristics. Chemosphere 247, 125811.
Pavagadhi, S., Tang, A.L.L., Sathishkumar, M., Loh, K.P., Balasubramanian, R., 2013. Removal of microcystin-LR and microcystin-RR by graphene oxide: adsorption and kinetic experiments. Water Res. 47, 4621–4629.
Rastogi, R.P., Sinha, R.P., Incharoensakdi, A., 2014. The cyanotoxin-microcystins: current overview. Rev. Environ. Sci. Biotechnol. 13, 215–249.
Ren, S., Usman, M., Tsang, D.C., O-Thong, S., Angelidaki, I., Zhu, X., et al., 2020. Hydrochar-facilitated anaerobic digestion: evidence for direct interspecies electron transfer mediated through surface oxygen-containing functional groups. Environ. Sci. Technol. 54, 5755–5766.
Ren, J., Huang, H., Zhang, Z., Xu, X., Zhao, L., Qiu, H., et al., 2023. Enhanced microbial reduction of Cr (VI) in soil with biochar acting as an electron shuttle: crucial role of redox-active moieties. Chemosphere 328, 138601.
Salvador, F., Martin-Sanchez, N., Sanchez-Hernandez, R., Sanchez-Montero, M.J., Izquierdo, C., 2015. Regeneration of carbonaceous adsorbents. Part II: chemical, microbiological and vacuum regeneration. Microporous Mesoporous Mater. 202, 277–296.
Sharma, M., Khurana, H., Singh, D.N., Negi, R.K., 2021. The genus Sphingopyxis: systematics, ecology, and bioremediation potential-a review. J. Environ. Manag. 280, 111744.
Song, H.J., Gurav, R., Bhatia, S.K., Lee, E.B., Kim, H.J., Yang, Y.-H., et al., 2021. Treatment of microcystin-LR cyanotoxin contaminated water using Kentucky bluegrass-derived biochar. Journal of Water Process Engineering 41, 102054.
Teng, W., Wu, Z., Fan, J., Chen, H., Feng, D., Lv, Y., et al., 2013a. Ordered mesoporous carbons and their corresponding column for highly efficient removal of microcystin-LR. Energy Environ. Sci. 6, 2765–2776.
Teng, W., Wu, Z., Feng, D., Fan, J., Wang, J., Wei, H., et al., 2013b. Rapid and efficient removal of microcystins by ordered mesoporous silica. Environ. Sci. Technol. 47, 8633–8641.
Teng, W., Wu, Z., Fan, J., Zhang, W.-x., Zhao, D., 2015. Amino-functionalized ordered mesoporous carbon for the separation of toxic microcystin-LR. J. Mater. Chem. A 3, 19168–19176.
Tong, H., Hu, M., Li, F., Liu, C., Chen, M., 2014. Biochar enhances the microbial and chemical transformation of pentachlorophenol in paddy soil. Soil Biol. Biochem. 70, 142–150.
Tran, H.N., 2022. Improper estimation of thermodynamic parameters in adsorption studies with distribution coefficient KD (qe/Ce) or Freundlich constant (KF): considerations from the derivation of dimensionless thermodynamic equilibrium constant and suggestions. Adsorpt. Sci. Technol. 2022, 0–23.
Tseng, R.-L., Wu, F.-C., 2008. Inferring the favorable adsorption level and the concurrent multi-stage process with the Freundlich constant. J. Hazard. Mater. 155, 277–287.
Wang, G., Gao, X., Li, Q., Zhao, H., Liu, Y., Wang, X.C., et al., 2020. Redox-based electron exchange capacity of biowaste-derived biochar accelerates syntrophic phenol oxidation for methanogenesis via direct interspecies electron transfer. J. Hazard. Mater. 390, 121726.
Weber, K., Quicker, P., 2018. Properties of biochar. Fuel 217, 240–261.
Wei, L., Lu, J., 2021. Adsorption of microcystin-LR by rice straw biochars with different pyrolysis temperatures. Environ. Technol. Innov. 23, 101609.
Wei, J., Pengji, Z., Zhang, J., Peng, T., Luo, J., Yang, F., 2023. Biodegradation of MC-LR and its key bioactive moiety Adda by Sphingopyxis sp. YF1: comprehensive elucidation of the mechanisms and pathways. Water Res. 229, 119397.
WHO, 2020. Cyanobacterial Toxins: Microcystins. World Health Organization Geneva, Switzerland.
Wurtsbaugh, W.A., Paerl, H.W., Dodds, W.K., 2019. Nutrients, eutrophication and harmful algal blooms along the freshwater to marine continuum. Wiley Interdiscip. Rev. Water 6, e1373.
Xiao, C., Yan, H., Wang, J., Wei, W., Ning, J., Pan, G., 2011. Microcystin-LR biodegradation by Sphingopyxis sp. USTB-05. Frontiers of Environmental Science & Engineering in China 5, 526–532.
Yan, H., Wang, H., Wang, J., Yin, C., Ma, S., Liu, X., et al., 2012. Cloning and expression of the first gene for biodegrading microcystin LR by Sphingopyxis sp. USTB-05. J. Environ. Sci. 24, 1816–1822.
Yang, F., Huang, F., Feng, H., Wei, J., Massey, I.Y., Liang, G., et al., 2020. A complete route for biodegradation of potentially carcinogenic cyanotoxin microcystin-LR in a novel indigenous bacterium. Water Res. 174, 115638.
Yu, L., Yuan, Y., Tang, J., Wang, Y., Zhou, S., 2015. Biochar as an electron shuttle for reductive dechlorination of pentachlorophenol by Geobacter sulfurreducens. Sci. Rep. 5, 16221.
Zeng, S., Kan, E., 2021. Adsorption and regeneration on iron-activated biochar for removal of microcystin-LR. Chemosphere 273, 129649.
Zeng, S., Kan, E., 2022. Thermally enhanced adsorption and persulfate oxidation-driven regeneration on FeCl3-activated biochar for removal of microcystin-LR in water. Chemosphere 286, 131950.
Zhang, H., Zhu, G., Jia, X., Ding, Y., Zhang, M., Gao, Q., et al., 2011. Removal of microcystin-LR from drinking water using a bamboo-based charcoal adsorbent modified with chitosan. J. Environ. Sci. 23, 1983–1988.
Zhang, S., Du, X., Liu, H., Losiewic, M.D., Chen, X., Ma, Y., et al., 2021. The latest advances in the reproductive toxicity of microcystin-LR. Environ. Res. 192, 110254.
Zhang, L., Tang, S., Jiang, S., 2023. Immobilization of microcystin by the hydrogel–biochar composite to enhance biodegradation during drinking water treatment. ACS Es&t Water 3, 3044–3056.
Zhao, Y., Li, J., 2022. Effect of varying pH and co-existing microcystin-LR on time-and concentration-dependent cadmium sorption by goethite-modified biochar derived from distillers' grains. Environ. Pollut. 307, 119490.